Building Simulation 2005

Ninth International IBPSA Conference
Montréal, Canada
August 15-18, 2005

SIMULATION OF STEADY-STATE NATURAL CONVECTION USING CFD

Tobias Zitzmann[1], Malcolm Cook[2], Peter Pfrommer[1],
Simon Rees[2], Ljiljana Marjanovic[2]
[1]University of Applied Sciences Coburg, Germany, [2]Institute of Energy and Sustainable Development, De Montfort University, Leicester, UK
Email: zitzmann@fh-coburg.de, Tel: +49 9561 317 302
Email: mcook@dmu.ac.uk, Tel: +44 116 257 7969

ABSTRACT

This paper investigates the air flow and heat transfer over a heated vertical plate and in a differentially-heated cavity using Computer Fluid Dynamics (CFD).

Parametric studies have been carried out to investigate the influence of near wall mesh density on air flow and heat transfer for natural-convection. Benchmark models have been used for steady-state simulations of laminar and turbulent free-convection flow for different turbulence models. Results have been validated with experimental data (Tian et al, 2001) and analytical predictions (Ostrach, 1956).

Appropriate meshing parameters and turbulence models were found which gave results which agreed well with the experiment and analytical data.

Key words: CFD, free convection, buoyancy, turbulence, heat transfer, Nusselt number, cavity

INTRODUCTION

A large part of building energy consumption world wide results from air-conditioning, mechanical ventilation and mechanical cooling. To achieve a comfortable interior climate without high energy demanding cooling components the building fabric is often used. For example, in the night-time cooling concept the solar and internal heating loads absorbed into the fabric during the day are re-emitted to the room and exhausted out of the building during night-time ventilation. The simulation and evaluation of these strategies demands the correct prediction of heat transfer between the building structure and interior. The heat transfer depends on the velocity and temperature distribution in a room, especially in the wall boundary layer. Free convection is typically the main driving force of the flow. However, using CFD for modelling these flows in enclosures is difficult since the buoyancy forces produce a weak coupling between the enthalpy and v-momentum equations, and accurately predicting the heat transfer coefficient at the surface is highly dependent on the mesh size. Very little literature is available which offers guidance on how to model buoyancy-driven flows using unstructured meshes in CFD, since most authors used structured mesh in the past (e.g. Peng and Davidson, 1999 and 2001, Thompson, Wilkes and Jones, 1985).

This paper provides guidelines on how to use CFD with unstructured meshes to model buoyancy-driven flow in a cavity. Benchmark CFD results are compared with published analytical data of Ostrach (1956), hereafter refered to as Ostrach, experiment data of Tian and Karayiannis (2001), hereafter refered to as TK, and numerical solutions of Berghein, Penot, Mergui and Allard (1993).

The paper is devided into three sections: 'Simulation Models', which gives details of the CFD code used and definitions of the boundary conditions; 'Results and Discussion', in which the comparisons between the CFD predictions and the analytical/experimental data are analysed; 'Conclusions', which summarize the most accurate method for modelling these flows with the CFD code used.

SIMULATION MODELS

Introduction to the CFD Solver

The CFD code used in this work uses CFX-5 (Ansys CFX (2003)) and is based on a finite volume method which uses an unstructured mesh containing tetrahedral and prism elements. This has the advantage that local numerical diffusion is reduced and is therefore suitable for complex flows with e.g. flow reversal. The code is based on a coupled solver for solving the differential equations using the fully implicit discretisation method and treating the hydrodynamic equations as one single system. To reduce the number of iterations required for convergence, a false-time stepping method is imposed which guides the approximate solutions in a physically based manner to a steady-state solution. Buoyancy is modelled using the Boussinesq approximation in which the forces are modelled as source terms in the momentum equations.

Various models exist in CFX-5 code for modelling turbulent flow. Two-equation models based on the eddy-viscosity concept include the k-ε (Launder and Spalding, 1974), k-ω (Wilcox, 1998) and Shear Stress Transport (SST) k-ω based (Menter, 1994)

models. Compared to the commonly used k-ε turbulence model, the k-ω model implies a new formulation for the near wall treatment which provides an automatic switch from a wall-function to a low-Reynolds number formulation based on the near-wall grid spacing. This makes it more accurate and more robust. The turbulence viscosity is assumed to be linked to the turbulence kinetic energy (k-equation) and turbulent frequency (ω-equation) instead of the turbulence dissipation rate (ε-equation in the k-ε model). To overcome the sensitivity of the k-ω model to freestream conditions, the SST model was developed. It blends the k-ω model near the surface with the k-ε model in the outer region.

In contrast, Reynolds Stress Turbulence models such as the standard Launder-Reece-Rodi Isotropic Production (LRR-IP) model (Launder et al, 1975) and Second Moment Closure-ω (SMC-ω) model (Wilcox, 1998), do not use the eddy-viscosity hypothesis, but solve transport equations for all components of the Reynolds stresses. This makes Reynolds Stress models more suited to complex flows. However, practice shows that they are often not superior to two-equation models because convergence difficulties often occur. The LRR-IP model is based on the k-ε model, whereas the SMC-ω is based on the k-ω model with the advantages already explained.

Benchmark 1: Quasi-2D-model for laminar flow over a heated vertical plate

The numerical model contained a 33°C isothermal wall of 381mm height. An adjacent ambient flow domain of 76mm width and an additional adiabatic wall and part of the ambient region at the low end of the isothermal heated wall (Figure 1) were imposed to allow sufficient space to avoid the surrounding boundaries influencing the results. 'Opening' boundaries were placed at the top the bottom and the right vertical boundary to allow air to flow in both directions depending on the pressure field. An ambient temperature of 21°C and zero velocity vector field were imposed for initial domain conditions and the 'opening' inflow. For this model a Rayleigh number of $Ra=3.9x10^5$ was calculated which indicates a purely laminar flow. Since the flow is two-dimensional, a 'symmetry' boundary condition with a model thickness of 10mm was chosen for the front and back of the domain. The walls and the core consisted of tetrahedral and triangular finite elements (see Figure 1) with maximum element edge length of 10mm to achieve high resolution. At the interface region between the isothermal and adiabatic wall the mesh was refined to increase the resolulution where the wall boundary layer begins to develop. Based on the equation of Yang and LaValle (2002) a maximum thermal boundary layer thickness of 21mm was calculated for the top end of the heated vertical plate. A sufficient nodal resolution in the wall boundary layer region (at least 15 nodes with the first node within $y+\leq 2$, as recommended by the code developers) required the use of prisms.

The influence of mesh resolution on temperatures and velocities in the wall boundary layer and on heat transfer at the heated plate was investigated by varying three key parameters for prism layer sizing: first prism size (use of 0.1mm, 0.2mm, 0.4mm, 1.0mm and 2.0mm), core prism size (use of 1.33mm, 2mm, 3mm and 4mm) and prism inflation (use of 1.5, 2.0 and 2.5). For investigations of constant core prism scales (by setting the prism inflation factor to unity) and prism inflation, a first prism size of 0.1mm was used (see Figure 2). In the sensitivity study of first prism sizes a constant core prism scale of 2.0mm was chosen. The first prism size determines the prism edge length in conversed direction of the surface normal for the first prism layer adjacent to the wall. The core prism size determines the prism edge length for the other prism elements towards the edge of the wall boundary layer and the outer region. A high mesh quality with finite element scales similar to the neighbouring elements reduces the risk of convergence problems. Therefore, with prism inflation the prism layer size can be increased gradually towards the core such that the last prism layer size has a similar scale to the edges of the neighbouring tetrahedral elements.

Results for benchmark 1 at y=380mm are compared with analytical work of Ostrach who derived expressions for velocity and temperature laminar wall boundary layer profiles at any height of a heated vertical plate. Ostrach's work was validated using data obtained from experiments of Schmidt and Beckmann (1930).

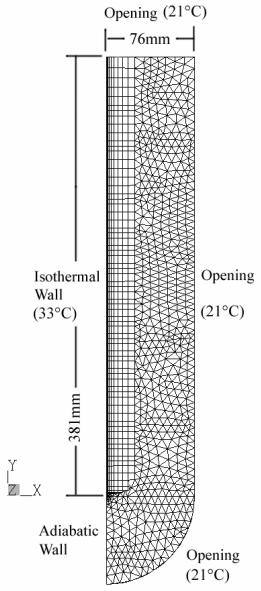

Figure 1: Numerical model for laminar flow at a heated vertical plate (benchmark 1).

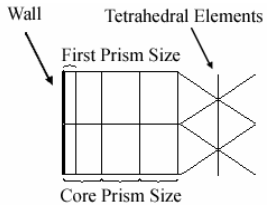

Figure 2: Near wall grid sizing

Benchmark 2: Quasi-2D-model for turbulent flow in a differentially heated cavity

This benchmark is based on experimental work carried out by TK. A cube with dimensions of X=750mm and Y=750mm and depth of Z=10mm was used for a quasi 2-D geometry. Constant temperatures of T_{Cold}=10°C and T_{Hot}=50°C were used at the isothermal vertical walls (Figure 3) for which a Rayleigh number of Ra=1.56x10^9 was calculated. Initial conditions of a zero velocity flow field and a homogeneous temperature of 30 °C were chosen for the fluid domain. In experiments adiabatic conditions are difficult to achieve. Therefore TK published the temperature profiles for the horizontal walls obtained in his experiments for adoption into numerical models which were used here for T_{Top} and T_{Bottom} (Figure 3). Since all wall boundary conditions have fixed temperature profiles and the absorption of radiation in the air was thought to be negligible, radiation effects were neglected. Hence no radiation model was used. Based on the results of benchmark 1, a mesh structure with a maximum surface and core mesh length scale of 10mm and 20mm, respectively, with mesh refinement in the corners was chosen. In the wall boundary layer (boundary layer thickness of 40mm at y/Y=0.5 based on Yang and LaValle) 13 prism layers with inflation factor 1.1 starting 1mm from the wall were positioned with two additional layers at 0.1mm and 0.5mm from the wall.

Using the geometry and boundary conditions described above, the four turbulence models k-ω, SST, LRR-IP and SMC-ω results were compared with experiments of TK.

Benchmark 3: 3D-model for turbulent flow in a differentially heated cavity

This was the same as benchmark 2, except the depth was extended to Z=375mm to analyse the influence of 3D effects on the results. The mesh was modified so that the elements were not refined at the corners. This was to keep the total number of elements within a practical limit for computing power. For the wall boundary layer 15 prism layers with an inflation factor of 1.2 starting at 0.5mm from the wall, with an additinal layer at 0.1mm from the wall, was used.

The most appropriate turbulence models for benchmark 2 were further used in benchmark 3 and results compared with experiments of TK.

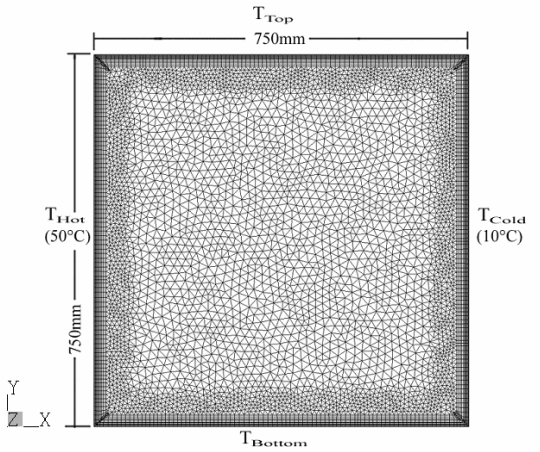

Figure 3: Numerical model for turbulent flow in a differentially heated cavity (benchmark 2).

RESULTS AND DISCUSSION

In the following figures the symbols on the interpolation are only for identification of the curves and do not represent nodes in the model. All data is plotted on the mid-depth line, z/Z=0.5 (V_0=1m/s is the buoyancy velocity). Solutions for benchmark 1 and 2 have converged to RMS (a root mean square residual) for the momentum equations of 10^{-7} and velocities remained constantly during the solution process at a certain monitoring point (except for the SMC-ω model). Each simulation required less than half a day for a Pentium 4, 2.55GHz machine. Simulations of benchmark 3 converged to RMS of 10^{-4} which is considered to have converged sufficiently as recommended by CFX. In contrast to the other benchmarks, steady-state values for benchmark 3 oscillated within a small range. Therefore, the results were statistically analysed and averaged over the oscillatory period. Each simulation required more than a week, which was clearly higher than for the quasi-2D models since 18 times more finite elements were used and more iterations were necessary for convergence.

BENCHMARK 1

Wall Boundary Layer

In Figure 4 the vertical velocity components and temperatures in the wall boundary layer at the top of the geometry at y=380mm close to the isothermal heated wall and average Nusselt numbers (Nu_{av}) are illustrated for different prism sizes. The vertical velocity components agreed well with the analytical solution of Ostrach for small 'core' prism sizes and deviated slightly with increased values at locations further away from the wall starting at about the velocity peak value (Figure 4a). For small 'first' prism sizes the velocities agreed well with the analytical solution and deviated only slightly between the wall and the location of the velocity

peak value as the prism size was increased (Figure 4b). Only the 2.0mm case showed significant deviations from the analytical solution. For various prism 'inflation factors' investigated the numerical solution agreed well with that of Ostrach between the wall and the location of the peak velocity value but deviated from there towards the core (Figure 4c). The deviation increased as the inflation factor was increased. The temperature profiles showed negligible deviation from the analytical solution for the prism scales investigated (compare Figures 4a-c).

Heat Transfer

Local heat transfer (indicated by local Nusselt numbers Nu_y) along the isothermal vertical plate was investigated. Nu_y deviated only marginally from the analytical solution for investigated prism scales and are hence not explicitly presented here in figures. Instead, the calculated average Nusselt numbers (Nu_{av}) for increased core prism sizes were compared with that of Ostrach for the isothermal surface (Figure 4d). For increased 'core' prism sizes a slight under-prediction of Nu_{av} existed. However, even for a prism size of 4.0mm the average Nusselt number only deviated from the analytical result by 2%. For a size of 2.0mm negligible deviation existed. The slightly higher average Nusselt number than that for the analytical results, for the potentially most accurate simulation (prism size of 1.33mm), may be caused by thermal effects from the adjacent adiabatic wall which are not present in the analytical model. An over-prediction was shown as the 'first' prism size was increased. For the tallest first prism size investigated (2.0mm) the average Nusselt number deviated from the analytical solution by 8%. Comparing average Nusselt numbers for core and first prism size variation the values were more sensitive to the first prism size, indicated by larger deviations. For prism 'inflation factors' investigated even the smallest factor investigated (1.5) over-predicted the average Nusselt Number by 2%.

Summary of Benchmark 1 Results

The parametric study showed that the temperature profile in the wall bounday layer might not change for a coarser wall boundary grid, although the air speeds and thus the heat transfer at the surface may be effected. Based on results for constant 'first' prism size of 0.1mm, core prism sizes of 2mm compared favourably well with the analytical solution. For constant 'core' prism sizes of 2mm, a first prism size of 0.2mm was found to be optimal for accurate predictions. However, results were more sensitive to the first prism size. In investigations with prism inflation, a small inflation factor gave best results. However, even the smallest factor investigated of 1.5 was too high to give results that agree exactly with experiment.

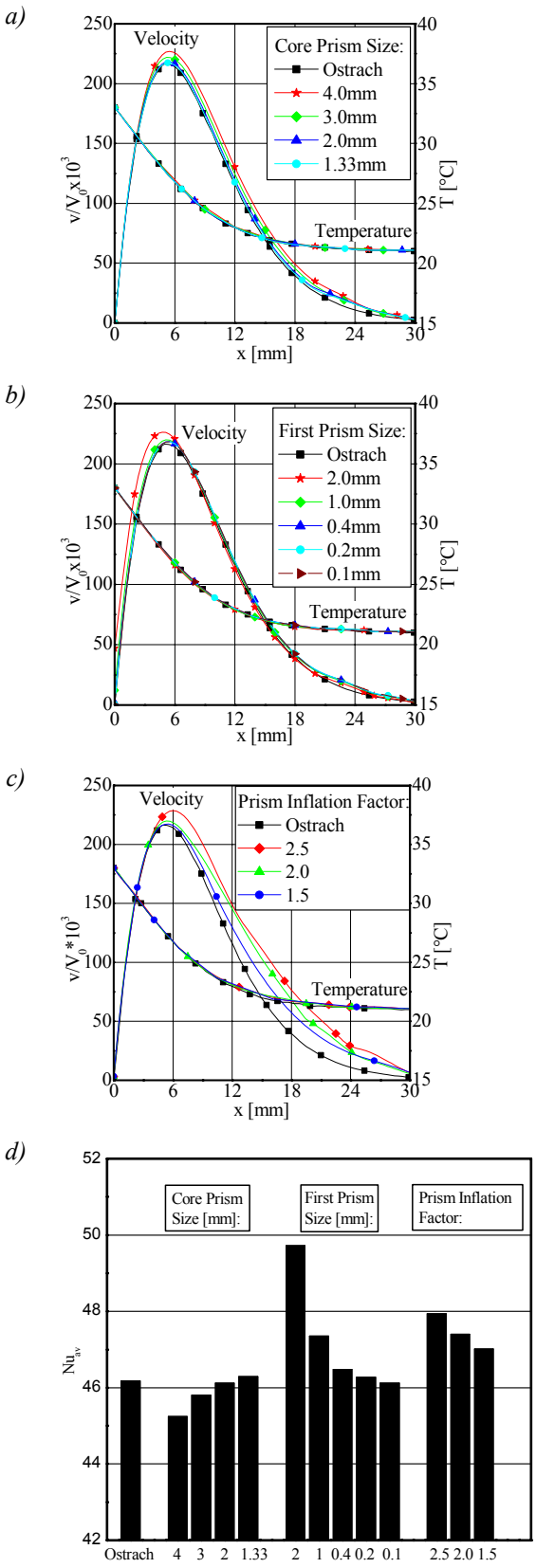

Figure 4: Comparison of predictions for various prism sizes with the analytical solution for y=380mm (benchmark1): a) Variation of prism sizes towards the core; b)Variation of wall adjacent prism sizes; c)Variation of prism inflation factors; d) average Nusselt numbers.

BENCHMARK 2

Wall Boundary Layer

Using the LRR-IP model the vertical velocity components and temperatures in the wall boundary layer at mid height of the space were significantly under-predicted (Figure 5a). When the SST model and SMC-ω were used the peak velocity was slightly over-predicted, temperatures were slightly under-predicted towards the cavity core. For the k-ω model, velocity and temperature profiles were in good agreement with experiments and deviated only for the peak velocity and temperatures further away from the wall.

Fluid properties at mid width

At mid width, deviation of differences between the temperature at mid height of the cavity and the peak temperature at the low end and high end, respectively, indicate a small horizontal displacement of the measured values (Figure 5b). For the numerical models no horizontal displacement of temperature existed and the point symmetry to the mid point of the space was well predicted. However, except for LRR-IP model which showed significant under-prediction, simulations slightly over-predicted the temperature peaks. Closest agreement with the measurements was shown for the k-ω model.

For horizontal velocity components at mid width of the enclosure, the numerical models slightly under-predicted the measured main flow peak values (Figure 5c), except the SST model which favourably agreed adjacent to the lower wall. The LRR-IP model gave largest discrepancies. A flow reversal at cavity mid width was only shown by using the SMC-ω and SST model, but velocities were significantly under-predicted (Figure 5c).

A typical velocity vector plot for the cavity mid plane (z/Z=0.5), however, showed small regions of weak flow reversal for the k-ω model further away from the mid width (Figure 6a), which therefore was not visible in figure 5c. The deviation of reversal regions were thought to be due to two flow disturbances in the bottom-right and top-left corners (Figure 6a), which were not visible in the experiments of TK (see Figure 6b). The reason for these disturbances was thought to be the use of a shallow geometry in benchmark 2 which prohibited 3D effects of turbulence being dissipated. Additional investigations with a higher numerical resolution (10mm core element edge scale) resulted in larger regions of flow reversal, however, under-prediction still existed. Since the higher resolution would exceed the practical limit for computer power and results are only marginally better for the prediction of the flow reversal, this was not investigated further.

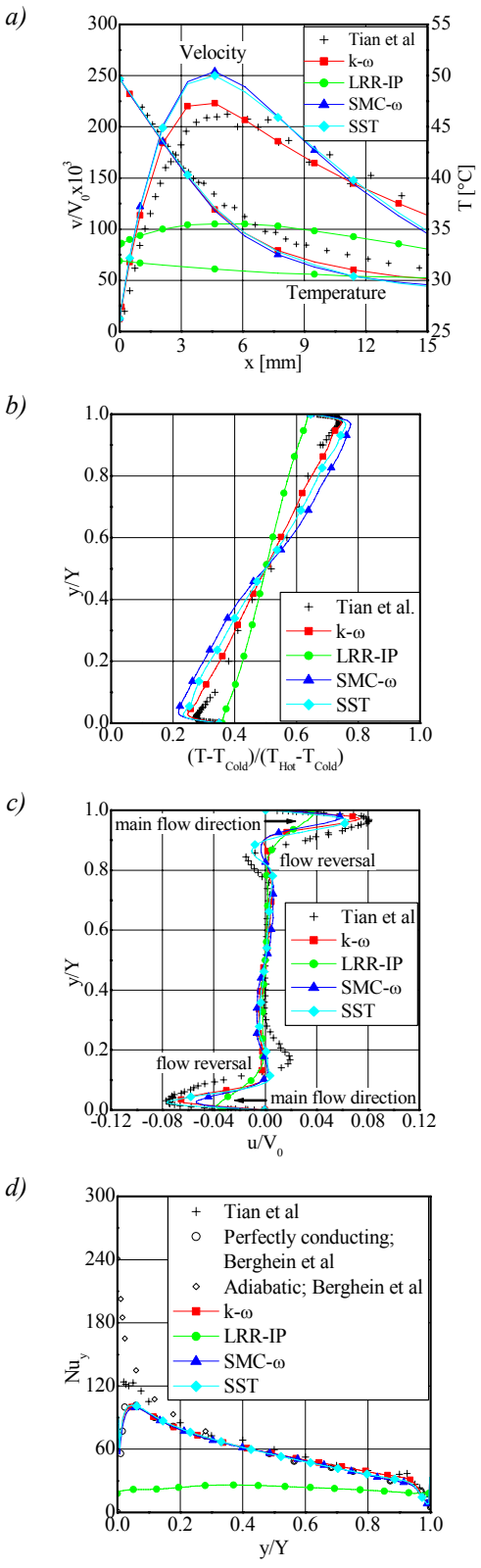

Figure 5: Comparison of predictions for various turbulence models with experiments (benchmark 2): a) Vertical velocity components and temperatures at y/Y=0.5; b) temperatures at x/X=0.5; c) horizontal velocity components at x/X=0.5; d) local Nusselt numbers at x/X=0.

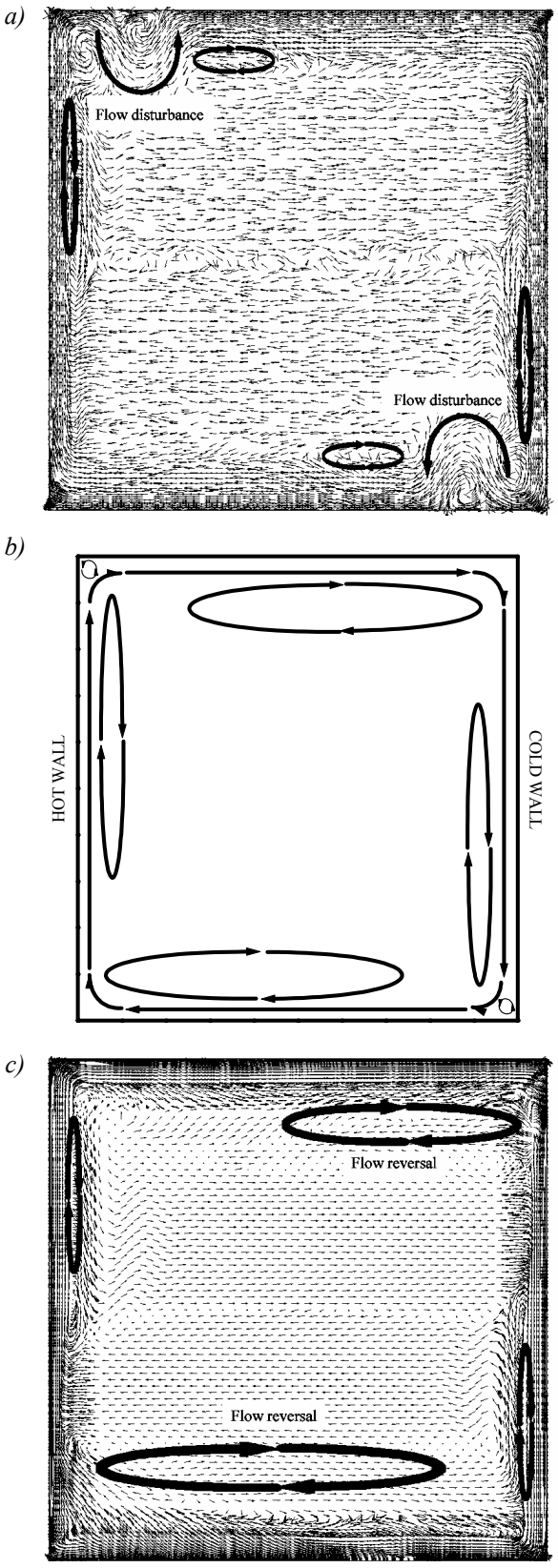

Figure 6: Flow fields: a) vector plot for benchmark 2 using the k-ω model; b) schematic of the flow field showing recirculation regions as observed by TK (2001); c) vector plot (for a selected iteration step) for benchmark 3 using the k-ω model.

Heat Transfer

The heat transfer from the hot vertical wall for different turbulence models are compared with experiments of TK and numerical solutions of Berghein et al (1993) for adiabatic and perfectly conducting horizontal wall boundary conditions (for $Ra=1.34x10^9$) in Figure 5d. The Nusselt numbers for the turbulence models investigated (except LRR-IP) followed the perfectly conducting curve shape of Bergein et al since the horizontal boundaries acted as perfectly conducting conditions because of the profiles carried over from TK. The numerical solutions were in good agreement with experiments between mid height and top of the enclosure. Towards the bottom experiments lay somewhere between the numerical solutions of Bergein et al.

Summary of Benchmark 2 Results

Numerical investigations with benchmark 2 agreed qualitatively with published experimental data for turbulent free-convection. The k-ω and SST turbulence model gave the most favourable agreement with experimental work. However, flow reversal near the horizontal walls which existed in the experiments was under-predicted using the CFD model. This was thought to be due to flow disturbances predicted in the corners of the geometry (Figure 6a) caused by the quasi two-dimensional geometry in which the close proximity of the symmetry planes prohibited airflow in all directions.

BENCHMARK 3

In benchmark 3 the k-ω and SST turbulence models were further investigated as they provided the most accurate results for benchmark 2.

Wall Boundary Layer

Both turbulence models over-predicted the peak velocity (Figure 7a); the k-ω model gave results closest to the experiment. The temperature profiles were slightly under-predicted towards the cavity core by both turbulence models.

Fluid properties at mid width

The numerical solution for temperatures at mid width of the cavity showed a well predicted point symmetry to the mid point of the space for both turbulence models (Figure 7b). Discrepancies existed in the temperature profile and the peak temperature values were slightly over-predicted. Although the temperature curve shapes of both turbulence models agreed quantitatively in the core, the peaks predicted with the k-ω model were closer to the experiments.

Flow reversal was shown by both turbulence models in the plot of horizontal velocity components at mid width of the enclosure (Figure 7c), although it was significantly under-predicted by both (except for the

k-ω model at the lower end, where it was well predicted). The k-ω model slightly underpredicted the peak velocities of the main flow, whereas the SST model agreed well with the experiments. In the core region the velocities were slightly higher for both turbulence models than in the experiments. Flow disturbances in the corners as predicted in benchmark 2 did not exist in benchmark 3 and the reversal flow regions shown in the velocity vector plots (e.g. the the k-ω model, Figure 6c) are comparable with those of TK (Figure 6b).

Heat Transfer

Results for local Nusselt numbers at the hot vertical wall agreed well with the experiments and the numerical results of Berghein et al towards the top of the cavity (Figure 7d). However, Nusselt numbers were under-predicted towards the bottom of the cavity for both turbulence models. In contrast to benchmark 2 no element refinement was used in the corners of benchmark 3. Based on the horizontal wall temperature profiles of TK the temperatures at both ends of the horizontal walls deviate slightly from the adjacent vertical wall temperatures. Thus a greater heat flux was caused at the interface than for benchmark 2 which is indicated by the Nusselt number peaks near the horizontal walls in Figure 7d. At mid height the local Nusselt numbers predicted using the k-ω model were closer to the measured data and solutions of Berghein et al than those using the SST model; at the low end the SST model showed better agreement.

Summary of Benchmark 3 Results

Numerical solutions of benchmark 3 results agreed qualitatively well with the experiments using the k-ω and SST model. The flow reversal was predicted for both cases. However, temperatures were slightly over-predicted for mid width and marginally under-predicted for the mid height of the cavity. The velocities were slightly over-predicted for mid height and under-predicted for the mid width of the space.

COMPARISON OF BENCHMARK 2 AND 3

For the fluid properties and heat transfer investigated, the results for velocity, temperature and Nusselt number were closer to the experiments using benchmark 2 than benchmark 3 for both turbulence models. However, using the k-ω model, the flow reversal regions were better predicted for benchmark 3 than benchmark 2. Furthermore, flow disturbances existed in the corners for benchmark 2 which did not appear in benchmark 3 which was thought to be caused by the close proximity of the symmetry planes. This suggested that the geometry depth of benchmark 3 was sufficient to allow flow at z/Z=0.5 to move in all directions without being influenced by the symmetry planes.

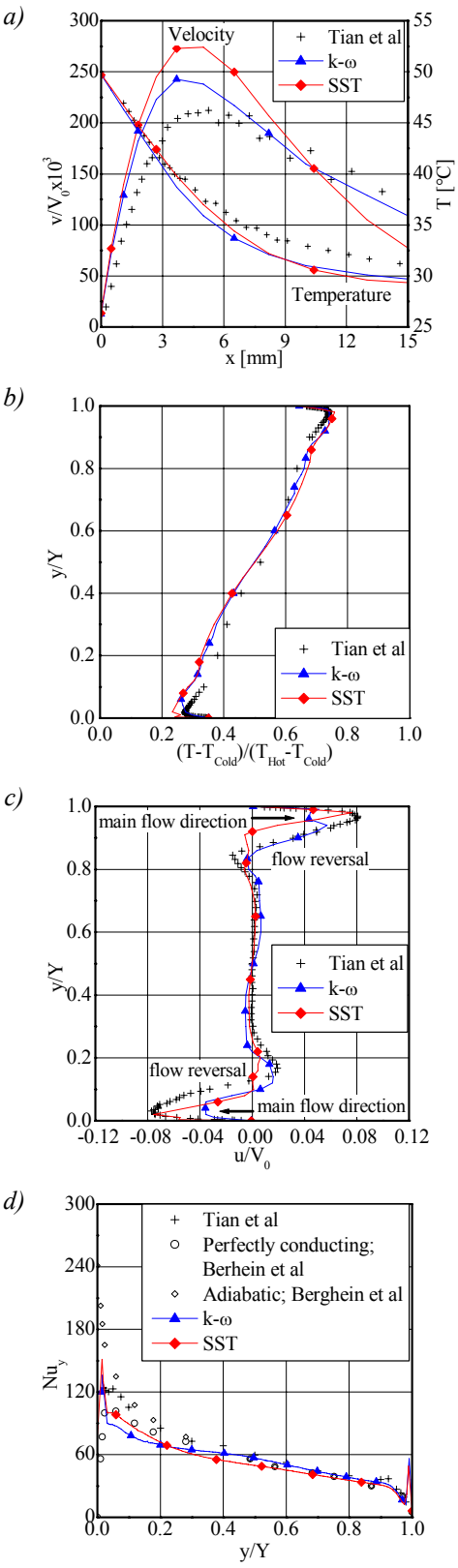

Figure 7: Comparison of predictions for selected turbulence models with experiments (benchmark 3): a) Vertical velocity components and temperatures at y/Y=0.5; b) temperatures at x/X=0.5; c) horizontal velocity components at x/X=0.5; d) local Nusselt numbers at x/X=0.

CONCLUSIONS

For the free convection flows studied in this work, it was found that prisms were required in the near wall region to accurately resolve the wall boundary layer. For the laminar case, the predicted numerical results for heat transfer, velocities and temperatures in the wall boundary layer agreed well with published analytical data. It was found that a maximum first prism size of 0.2mm and constant core prism sizes no larger than 2.0mm were required to obtain accurate results. Prism inflation might increase mesh quality and hence improve convergence. Initial investigations showed that the inflation factor should be at least lower than 1.5 for the cases considered.

For turbulent natural convection modelling, the mesh parameter settings were based on the results of benchmark 1. Results for different turbulence models to predict flow in a differentially heated cavity compared favourably with experiments using benchmark 2. Only the LRR-IP turbulence model deviated significantly from experiments; the SST and k-ω turbulence models predicted the most favourable results. However, velocity disturbances existed in the corners of the geometry where the flow impinged on the top or bottom of the space. A further investigation of the SST and k-ω models in 3D suggested that these deviations from measurements were caused by the close proximity of the symmetry planes which inhibited 3D dissipation of turbulence effects of the flow. Benchmark 2 (quasi-2D) compared well with the 3D case (benchmark 3) except for the flow disturbances which appeared in the cavity corners in the quasi-2D case. Both the k-ω and SST turbulence models gave favourable results for both benchmarks.

The investigations showed that CFX-5 has the capability to predict buoyancy-driven turbulent flow in a differentially-heated cavity.

NOMENCLATURE

α	thermal diffusivity [m^2/s]
β	thermal expansion coeff. [1/K]
ε	turbulence eddy dissipation [m^2/s^3]
g	gravity [m/s^2]
k	turbulence kinetic energy [m^2/s^2]
Nu_{av}	average Nusselt Number [-]
Nu_y	local Nusselt No. [-], $=0.386Ra^{0.25}y^{-0.25}$
Ra	Rayleigh No. [-], $=g\beta(T_{Hot}-T_{Cold})Y^3\alpha^{-1}\nu^{-1}$
T_{Top}, T_{Bottom}	temperature profiles at the top and bottom of the geometry [°C]
T_{Hot}, T_{Cold}	isothermal temperatures at the hot and cold vertical walls [°C]
u	horizontal velocity comp. [m/s]
u_τ	friction velocity [m/s]
v	vertical velocity comp. [m/s]
ν	kinematic viscosity [m^2/s]
V_0	buoyant velocity [m/s], $=(g\beta\Delta TY)^{-0.5}$
X, Y, Z	geometry dimensions [mm]
x, y, z	local dimensions for analysis [mm]
ω	turbulence frequency [1/s]
y+	normalised wall distance [-], $=\Delta y u_\tau/\nu$

REFERENCES

Ansys CFX, 2003: CFX-5 Solver Models and Theory User Manuals, Version 5.6.

Berghein C., Penot F., Mergui S., Allard F., 1993: Numerical and experimental evaluation of turbulent models for natural convection simulation in a thermally driven square cavity, Proc. ASME Conf., pp 1-12.

Launder B.E., Spalding D.B., 1974: The numerical computation of turbulent flows, Comp. Meth. in Applied Mech. Eng., Vol 3, pp 269-289.

Launder B., Reece G. and Rodi W., 1975: Progress in the development of a Reynolds-stress turbulence closure, J. Fluid Mech., Vol 68 (3), pp 537-566.

Menter, F.R., 1994: Two-equation eddy viscosity turbulence models for engineering applications, AIAA Journal, Vol 32 (8), pp. 1598-1605.

Ostrach S., 1953: An analysis of laminar free-convection flow and heat transfer about a flat plate parallel to the direction of the generating body force, NACA, Report 1111, Madison.

Peng S.-H., Davidson L., 1999: Computation of turbulent buoyant flows in enclosures with low-Reynolds-number k-ω models, Int J. Heat Fluid Flow, Vol 20, pp 172-184.

Peng S.-H., Davidson L., 2001: Large eddy simulation for turbulent buoyant flow in a confined cavity, Int. J Heat Fluid Flow, Vol 22, pp 323-331.

Schmidt E. and Beckmann W., 1930: Das Temperatur- und Geschwindigkeitsfeld vor einer Wärme abgebenden senkrechter Platte bei natürlicher Konvektion, Tech. Mech. Thermodyn., Bd 1 (10 u 11), Germany.

Thompson C.P., Wilkes N.S. and Jones I.P., 1987: Numerical studies of buoyancy-driven turbulent flows in a rectangular cavity, Int. J. Num. Meth. Eng., Vol 24, pp89-99.

Tian J., Karayiannis T.G., 2001: Low turbulence natural convection in an ait filled square cavity, Part 1: the thermal and fluid flow fields, J. Heat and Mass Transfer, Vol 43, pp 849-866.

Wilcox D.C., 1998: Turbulence modeling for CFD, 2nd edn., DCW Industries Inc., Canada.

Yang R., LaValle P., 2002: Heat transfer by natural convection, Course Script, Uni. of Michigan.